Int. J. Multiphase Flow Vol. 13, No. 6, pp. 785–802, 1987
Printed in Great Britain.

0301-9322/87 $3.00 + 0.00

EFFECTS OF VORTEX PAIRING ON PARTICLE DISPERSION IN TURBULENT SHEAR FLOWS

R. CHEIN and J. N. CHUNG
Department of Mechanical and Materials Engineering, Washington State University, Pullman, WA 99164-2920, U.S.A.

(*Received* 1 *May* 1986; *in revised form* 10 *June* 1987)

Abstract—Particle dispersion in large-scale dominated turbulent shear flow is investigated numerically with special emphasis on the effects of the vortex-pairing phenomenon. The particle dispersion is visualized numerically by following the particle trajectories in a flow consisting of large vortices which are undergoing pairing interaction. The flow field is generated by a discrete vortex method. Important global and local flow quantities from the numerical simulation compare reasonably well with experimental measurements.

For both cases of point sources with continuous particle release and an initially distributed line source, the particle dispersion results demonstrate that the extent of particle dispersion depends strongly on the Stokes number, the ratio of the particle aerodynamic response time to the characteristic time of the vortex-pairing flow field. Particles with relatively small Stokes numbers disperse laterally at approximately the same rate as that of the fluid particles and particles with large Stokes numbers disperse much less than the fluid particles. Particles with intermediate Stokes numbers (0.5–5) may be dispersed laterally farther than the fluid particles and may actually be flung out of the vortex structures. Due to the strong particle entrainment power, the flow during the vortex-pairing process seems to produce higher particle lateral dispersion than the pre-pairing and post-pairing flows.

1. INTRODUCTION

Particle dispersion by turbulent shear flows is of importance, for example, in liquid fuel spray combustion, pulverized coal combustion and many energy-related processes. The dispersion of fuel droplets caused by the fluid turbulence is a dominant factor that affects the stability and performance of a combustor. A coal-fired power plant relies on the proper dispersion of particles in the feed jets to provide a well-mixed gas–particle flow for efficient combustion. The proper design of these flow processes depends heavily on the understanding of the interactions of particles with the turbulent flow structures.

The dispersion of particles in turbulent flows has received some attention only in certain types of turbulence. The traditional approach is to regard the process as a Fickian diffusion process and to quantify the mass transfer of particulates by a diffusion coefficient and a particle concentration gradient. This model may be adequate for near-isotropic turbulent flows such as that generated by a grid; however, the majority of particle mixing and dispersion problems involve shear-driven turbulent flow in which the mean velocity gradient produces non-isotropic large-scale turbulent structures.

Recent breakthroughs in turbulent flow research have demonstrated that turbulent flow driven by an asymmetric velocity gradient, such as mixing layers, jets and wakes, contains quasi-orderly large-scale structures (Brown & Roshko 1974; Winant & Browand 1974; Yule 1980). Brown & Roshko's (1974) shadowgraphic pictures of mixing layers between dissimilar gases clearly indicated the existence of organized large-scale structures in the turbulent flow region. Winant & Browand's (1974) dye visualizations of a mixing layer between two water streams demonstrated that the growth and the momentum transport of the mixing layer were controlled totally by the interactions of these large-scale structures. They also discovered that the basic mechanism of large-scale structure interactions is through the "pairing" of two adjacent large vortex structures of similar size. After rotating around each other, these two vortices will gradually merge and eventually lose their original identities to form a single structure twice the size of the former two. This process also explains the growth mechanism of a mixing layer. The measurements of Browand & Weidman (1976) confirmed that these structures consist of concentrated vortices. Based on their mea-

surements, Browand & Troutt (1980, 1985) reported that large-scale structures in a mixing layer are basically two-dimensional in nature and the bulk of the momentum carried by the fluid is, accordingly, also two-dimensional. Since the large-scale vortex structures carry most of the momentum in a shear layer, it is reasonable to assume that large-scale structures are instrumental in controlling particle dispersion. Consequently, it is believed that the "pairing" process plays a dominant role in the particle dispersion mechanism in a turbulent shear layer. This hypothesis is further supported by Yule's (1980) experiments of liquid droplet dispersion in an air spray; he states

> "Small droplets closely followed the gas flow and given a good visualization of the large eddies. However larger droplets with their smaller drag/inertia ratios, are seen to leave these eddies and penetrate the outer potential flow. Realistic modeling of drop environments and thus vaporization and burning, requires modeling of these large eddies and their interactions with the droplets."

Based on the above suggestions (Yule 1980), the current study is intended to provide such a modeling for large-scale eddies and their interactions with the particles.

As also pointed out by Yule (1980), the ratio of drag to inertia determines the extent to which particle motion will be influenced by the turbulent structures. Another way of representing the ratio of drag to inertia is through the ratio of the aerodynamic response time of the particle to a characteristic time scale of the large flow structures, as suggested by Gore *et al.* (1985). The aerodynamic response time of a particle is defined as $\tau_A = \rho_p d_p^2/18\,\mu$, where ρ_p is the particle density, d_p is the particle diameter and μ is the fluid viscosity. This quantity represents the time required for a particle, released from rest in a uniform flow, to reach 63% of the flow velocity (provided Stokes' drag law is applicable). It is simply a measure of the aerodynamic responsiveness of a particle. The time scale of the large vortex structure in the mixing layer, for example, may be approximated by $\tau_F = \delta/\Delta U$, where δ is the width of the mixing layer and ΔU is the velocity difference between the two free streams.

In this study, the ratio of the two time scales, τ_A/τ_F, also called the Stokes number, St (Crow 1982), is used to characterize the effectiveness of large-scale structures to move the particle laterally in a mixing layer. It is plausible to assume that for $St \gg 1$, the particles will not respond to the large eddies significantly and will exhibit little dispersion. For $St \ll 1$, the particles will follow closely the streamlines in the vortex structures and should disperse at the same rate as the mixing layer. For Stokes numbers ranging between these two extremes, particles may be captured by the vortex structures but eventually they may be flung out of the structure, as seen by Yule (1980). Depending on the values of the Stokes number that dictates the trajectory of a particle in a vortex structure, it is certainly possible for some of them to be flung beyond the boundary of momentum mixing region.

In summary, the bases for this paper are as follows: first, the momentum of a turbulent mixing layer is carried basically by two-dimensional large-scale vortex structures and "vortex pairing" is the dominant momentum transport mechanism that is responsible for the entrainment and growth of the mixing layer; second, the Stokes number is the key parameter for measuring the effectiveness of particle dispersion in large-scale vortex structures.

A discrete vortex method is adopted first to stimulate the vortex-pairing phenomena in a turbulent mixing layer. Quantitative particle dispersion in a vortex-pairing flow environment are then examined by numerically tracing their trajectories.

2. MATHEMATICAL MODEL

2.1. Flow-field simulation

As shown in the visualization pictures of Brown & Roshko (1974) and Winant & Browand (1974), a mixing layer is composed of an array of vortex pairs, as shown in figure 1, and every pair is undergoing pairing interactions. Also, each pair may be considered as a unit cell that constitutes the entire mixing layer except that for any adjacent units, the size of the unit on the downstream side is approximately twice that on the upstream side, as discovered by Winant & Browand (1974).

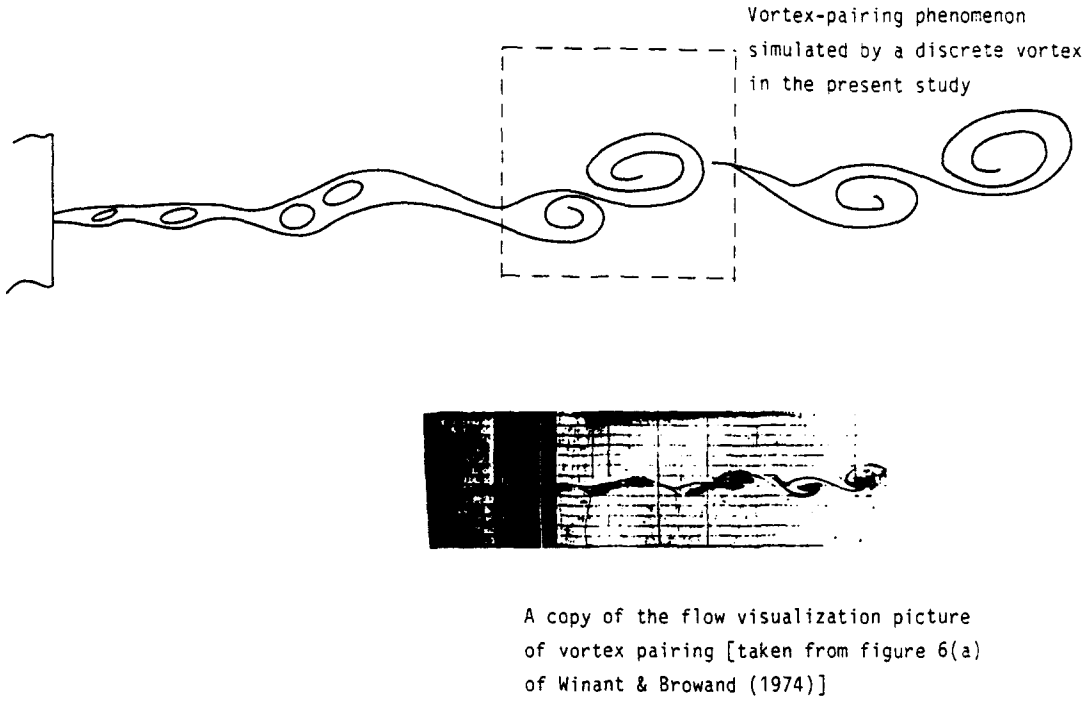

Figure 1. Vortex-pairing phenomenon in a turbulent mixing layer.

Due to the similarity in every aspect, except the size difference, between all the vortex pairs in a mixing layer, the current numerical simulation is designed to address only a typical pair, as marked by the dashed square in figure 1. The simulation starts with two separate identical vortices and continues through their pairing interaction until they merge to form a single vortex twice the size of the two initial vortices.

Discrete vortex simulation of turbulent flows, first proposed by Rosenhead (1932), has been successfully applied to a mixing layer (Ashurst 1979; Inoue 1985) and to a free jet (Acton 1980). In this study, the two initial large vortex structures and their pairing interactions are simulated by 96 discrete elementary vortices. Initially these elementary vortices arranged to form four identical sinusoidal rows, as shown in figure 2. Each row consists of two sinusoidal waves with wavelength λ. Two wavelengths are required to represent two large vortex structures and their subsequent pairing interactions. The amplitude of the sinusoidal wave and the separation distance between the rows are in general not sensitive parameters as long as they are relatively small, according to Acton (1976) who did a parametric study on these two parameters. In this study, the amplitude is set at 0.1 and the separation distance is 0.0975.

The essence of the discrete vortex method is that at any instant the flow field is determined by the superposition of the velocities induced by all discrete elementary vortices in the flow, therefore

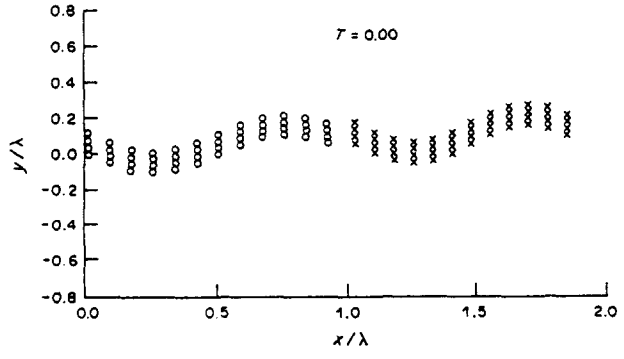

Figure 2. Initial distribution of vortices in the numerical model.

the locations and the strengths of all elementary vortices should be known in order to calculate the velocity distributions. In turn, the elementary vortices, which are equivalent to massless particles, are carried around by the flow field they induced. As a result, we need to specify the elementary vortices for the entire mixing layer not just for the vortex pair. One simple method to model a representative vortex pair, as suggested by Acton (1976), is to extend from this pair to both positive and negative infinities by repetition of this basic unit (two sinusoidal wavelengths shown in figure 2) in a cyclic array to form an infinite shear layer. In this manner, the results for this basic unit vortex pair will be free of boundary effects and truly representative of a typical unit structure. The stream function, $\psi(x, y)$, for the flow in a cycle of this infinite shear layer may be written as (Lamb 1945)

$$\psi(x, y) = \frac{1}{4\pi} \sum_{k=1}^{N_v} G_k \ln \left[\cosh\left(\frac{2\pi(y - y_k)}{a}\right) - \cos\left(\frac{2\pi(x - x_k)}{a}\right)\right], \quad [1]$$

where a is the length of this cycle; in this analysis, $a = 2\lambda$. N_v is the total number of vortices in this cycle; G_k and (x_k, y_k) are the strength and position of the k^{th} vortex, respectively. Accordingly, the induced velocity at any point (x, y) in a cycle of length a and N_v elementary vortices, which is a unit of an infinite row of repeating cycles, is given by

$$u(x, y) = \sum_{k=1}^{N_v} \frac{-G_k \sinh\left(\frac{2\pi(y - y_k)}{a}\right)}{2a\left[\cosh\left(\frac{2\pi(y - y_k)}{a}\right) - \cos\left(\frac{2\pi(x - x_k)}{a}\right)\right]} \quad [2]$$

and

$$v(x, y) = \sum_{k=1}^{N_v} \frac{G_k \sin\left(\frac{2\pi(x - x_k)}{a}\right)}{2a\left[\cosh\left(\frac{2\pi(y - y_k)}{a}\right) - \cos\left(\frac{2\pi(x - x_k)}{a}\right)\right]}. \quad [3]$$

Equations [2] and [3] are then applied to evaluate the velocity profiles in the cycle at any instant, depending on the distribution of vortices. Since each elementary vortex moves with the local velocity induced by the rest of the vortices in the system, the same velocity field is used to transport the massless vortices in the cycle. In numerical calculations of the vortex transport, a first-order integration scheme is involved. If (x_i^j, y_i^j) is the position of the ith vortex at $j\Delta t$ time (Δt is the time-step size), then the location of the ith vortex at $(j + 1)\Delta t$, (x_i^{j+1}, y_i^{j+1}), is calculated based on Euler's method as follows:

$$x_i^{j+1} = x_i^j + u(x_i^j, y_i^j)\Delta t \quad [4]$$

and

$$y_i^{j+1} = y_i^j + v(x_i^j, y_i^j)\Delta t, \quad [5]$$

where $u(x_i^j, y_i^j)$ and $v(x_i^j, y_i^j)$ are obtained from [2] and [3].

The reason for adopting the first-order Euler method is based on the justification given by Inoue (1985). The scheme requires much less computation time than other schemes of high-order accuracy. Recent investigations of the discrete vortex method have revealed that the numerical errors caused by the time integration introduce numerical viscous effects in the motion of vortices. As pointed by Kuwahara & Takami (1983), the numerical viscosity introduced as a result of numerical errors is actually similar to the effect of turbulent viscosity. The appropriateness of Euler's method in the current numerical integration is further supported by the satisfactory quality of the flow results shown in the Results and Discussion.

The strength of each vortex is assumed equal and is determined by

$$G_k = \frac{(\Delta U)2\lambda}{N_v}, \quad k = 1, 2, \ldots, 96, \quad [6]$$

where ΔU is the velocity difference between the two free streams of the mixing layer. In the current model, the upper free stream is moving at $-U$ and the lower free stream at U and therefore

$\Delta U = 2U$. A total of 96 vortices distributed along two wavelengths and in four rows was suggested by Acton (1980) and adopted in this analysis to give the shear layer a more detailed definition. In order to avoid the unrealistically high induced velocity when two elementary vortices come too close, the so-called vortex blob with a finite smooth core, suggested by Chorin (1973), is adopted for each elementary vortex in this calculation instead of point vortices.

In this numerical model, the length scale of the system is chosen to be the wavelength, λ_1 of the initial sinusoidal formation of the discrete vortices. It is noted that the size of the two initial large-scale vortices formed after the roll-up from the sinusoidal wave, is comparable to λ, as shown in figure 3. The characteristic time scale of the flow field is then defined as,

$$\tau_F = \frac{2\lambda}{\Delta U} = \frac{\lambda}{U}. \quad [7]$$

The dimensionless time is then given as

$$T = \frac{t}{\tau_F}. \quad [8]$$

All the velocities and lengths are non-dimensionalized by U and λ, respectively.

2.2. Particle dispersion

A Lagrangian approach to predict the particle motion in a mixing layer is detailed as follows. The trajectory of each particle in the flow is predicted directly from the equation of motion. The basic assumptions in the particle motion analysis are:

(1) all particles are rigid spheres with diameter d_p and density ρ_p;
(2) the density of the particles is assumed large compared to the density of the fluid;
(3) particle–particle interactions are neglected;
(4) the effect of the particles on the flow is neglected.

Based on the above assumptions it is generally accepted that the dominant force on each particle is the drag force from the ambient fluid (Cliff *et al.* 1978). Consequently, forces on the particles such as the virtual mass force, pressure gradient force and Basset force are neglected in this model.

The non-dimensional equation of motion for a particle according to the length and velocity scales chosen above can be written as

$$\frac{dV_p}{dT} = \frac{f}{St}(\mathbf{V} - \mathbf{V}_p), \quad [9]$$

where $\mathbf{V}_p$ is the dimensionless instantaneous particle velocity, $\mathbf{V}$ is the dimensionless instantaneous velocity of the fluid, f is the modifying factor for any deviation from the Stokes' drag and St is the Stokes number—defined as the ratio of the particle aerodynamic response time to the flow-field time scale:

$$St = \frac{\dfrac{\rho_p d_p^2}{18\mu}}{\dfrac{\lambda}{U}}, \quad [10]$$

μ is the fluid dynamic viscosity. The factor f is well-represented (Clift *et al.* 1978) for particle Reynolds numbers < 1000 by

$$f = 1 + 0.15\,Re_p^{2/3}, \quad [11]$$

where Re_p is defined as

$$Re_p = \frac{|\mathbf{V} - \mathbf{V}_p| d_p}{\nu}, \quad [12]$$

ν is the fluid kinematic viscosity. With the introduction of the flow-field Reynolds number, $Re = U\lambda/\nu$, and the non-dimensionalized particle size, $\gamma_d = d_p/\lambda$, [12] can be rewritten as

$$Re_p = |\mathbf{V} - \mathbf{V}_p| \gamma_d Re. \quad [13]$$

In [7], the Stokes number is related to the flow-field Reynolds number, the density ratio, $\lambda_\rho = \rho_p/\rho$ where ρ is the fluid density, and the non-dimensionalized particle size, γ_d:

$$\mathrm{St} = \tfrac{1}{18}\gamma_d^2\gamma_\rho \mathrm{Re}. \qquad [14]$$

In this analysis, the density ratios, based on those for gas–particle and gas–liquid droplet flows, range from 500 to 2500. For most types of actual flows, the Stokes number is usually of the order of unity, however, it could vary from as little as 10^{-2} to as large as 10^3, depending on the size and mass density of the particles. Since the flow simulation is based on the assumption of large Reynolds number inviscid flow, the choice of flow Reynolds number should be consistent with the flow assumption. In this analysis, the flow-field varies between 10^4 and 4×10^4.

It should be noted that according to [14], for a given Reynolds number and density ratio, each Stokes number value corresponds to a specific γ_d. Therefore, variation of the Stokes number represents the variation of dimensionless particle size in the calculation if Reynolds number and γ_ρ are held constant.

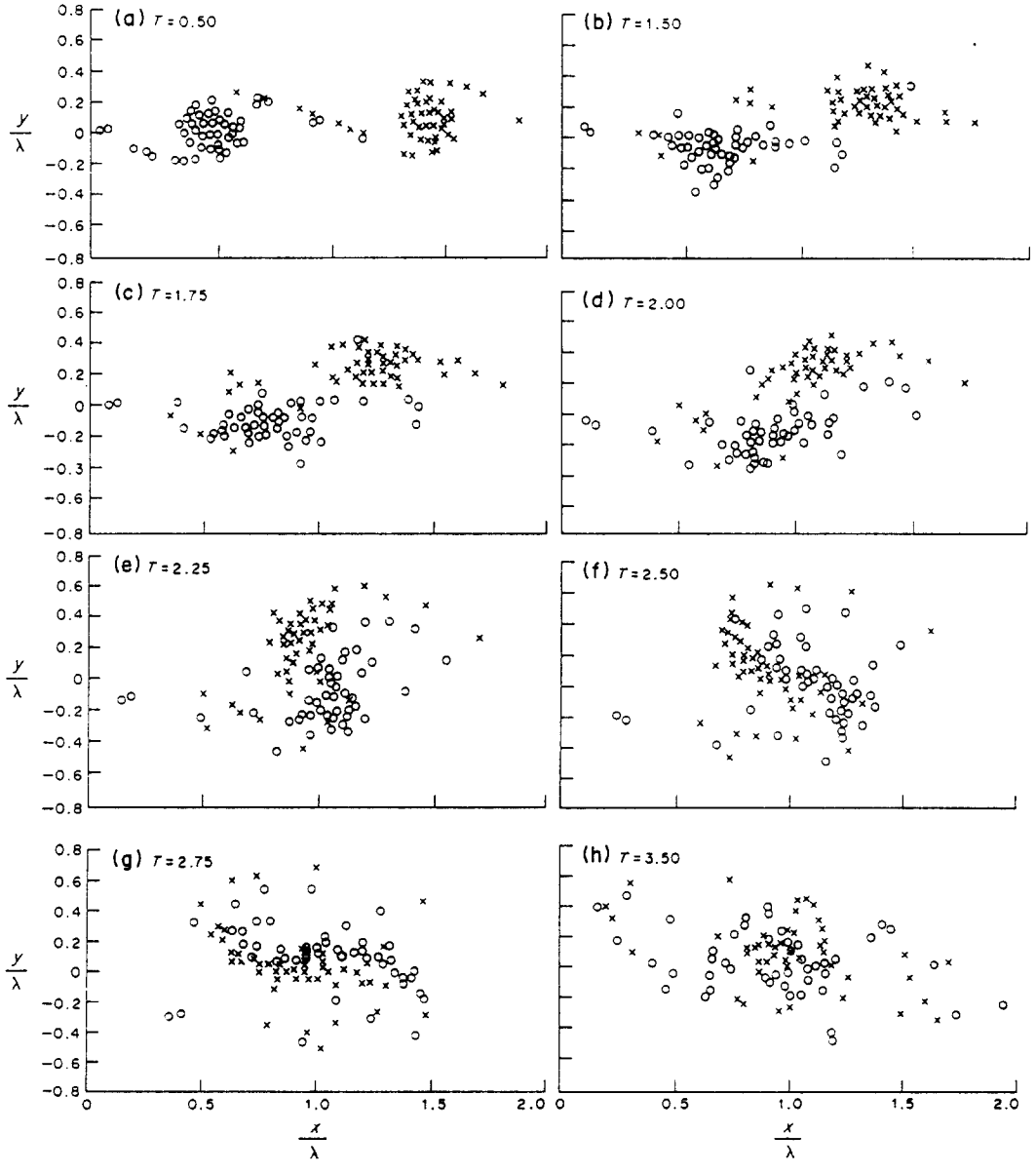

Figures 3(a–h). Development of the vortex-pairing process.

3. RESULTS AND DISCUSSION

First the flow-field solutions are presented. With starting positions as shown in figure 2 for all the vortices in the system, figures 3(a–h) show the subsequent development of the shear layer as a function of the dimensionless time. The two-wavelength sheets first roll up to form two separate large-scale structures, as shown in figure 3(a). Each is of the size of the wavelength λ. While the two large vortex structures are rotating about their own axes, they are also rotating around each other and begin to interact with each other. As the interaction continues, the two gradually coalesce and lose their individual identities. At $T = 3.0$, a larger single vortex, which is approximately twice the size of the two initial structures, is formed as a result of the coalescence of the original two

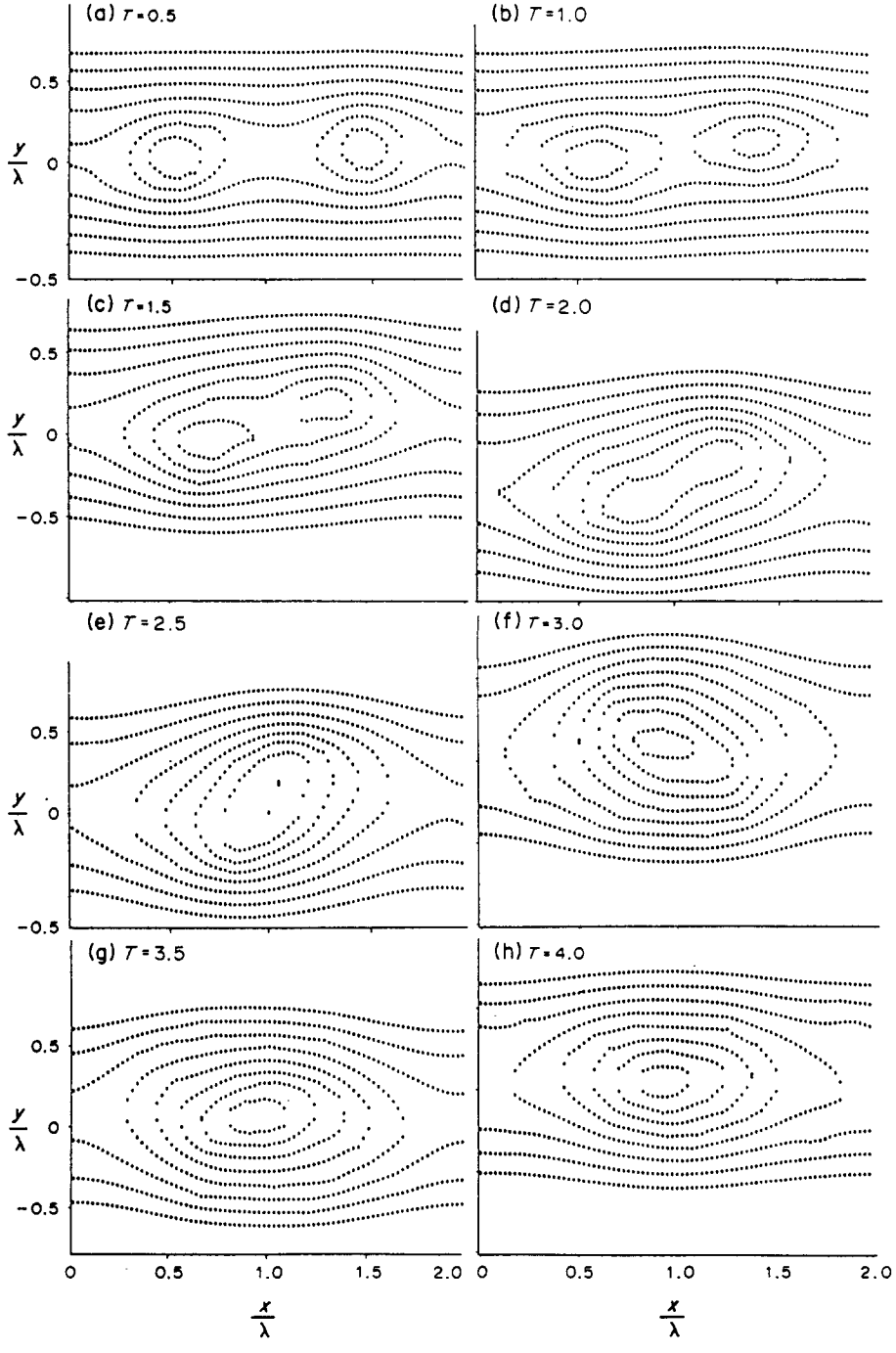

Figures 4(a–h). Streamlines at various stages during the flow development.

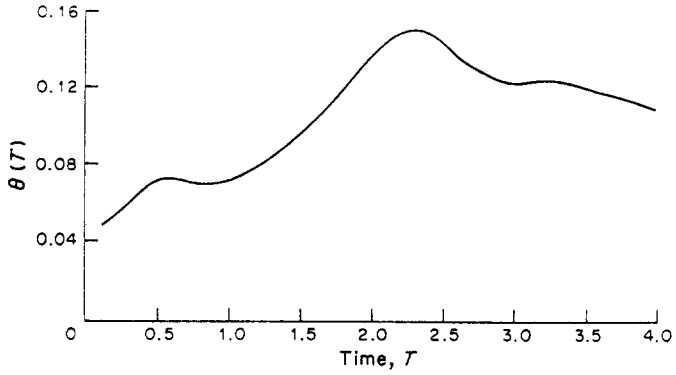

Figure 5. Variation of momentum as a function of time.

smaller vortex structures. This process is called the "pairing" process, as reported by Winant & Browand (1974). More qualitatively, we computed and plotted the streamlines at various stages during the pairing interaction in figure 4(a–h). It clearly supports the above assessment of the pairing process.

Due to the turbulent nature of the flow, it is important to present the time-averaged quantities of the flow field. Ordinarily, the time-averaged quantities are defined in an Eulerian coordinate system where time averaging is performed on a variable, such as velocity, at a fixed location. In the current Lagrangian modeling, the coordinates are fixed with the typical vortex pair, while in Eulerian coordinates, this typical vortex pair will be convected downstream. Therefore the

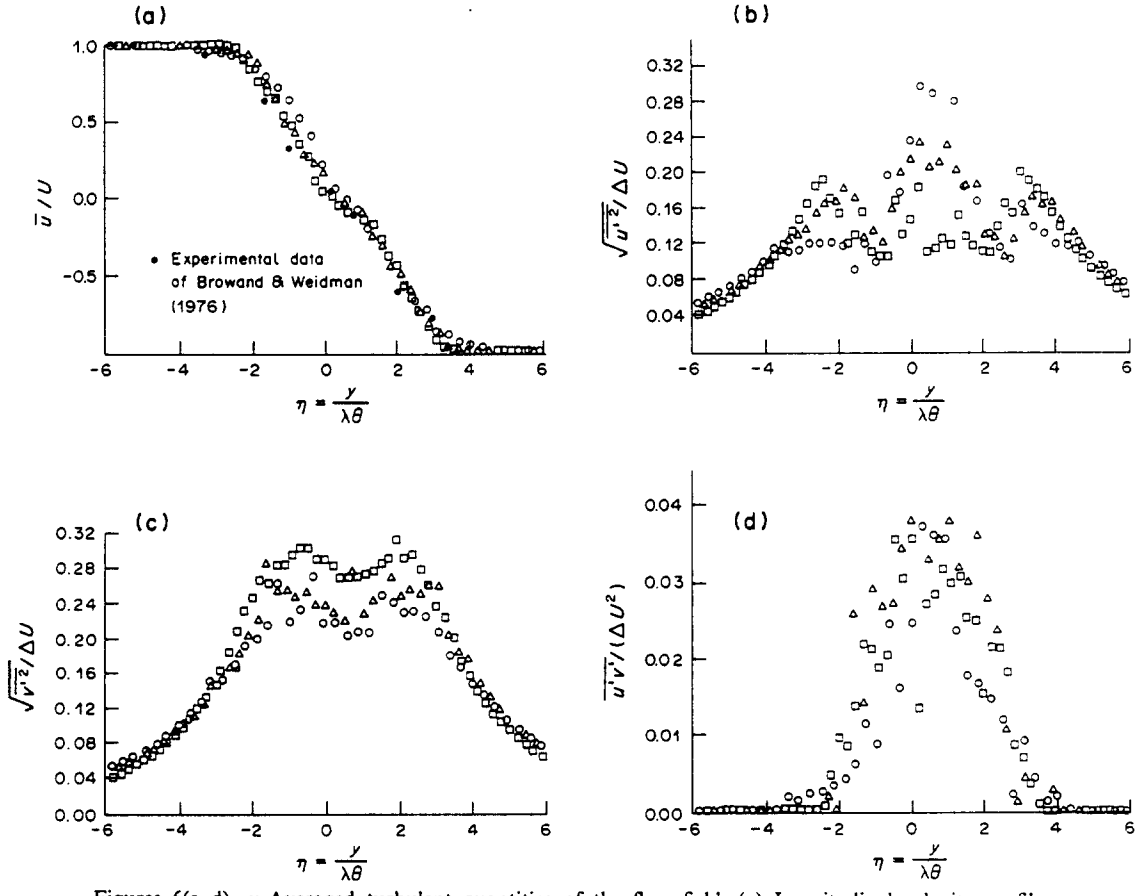

Figures 6(a–d). x-Averaged turbulent quantities of the flow field. (a) Longitudinal velocity profiles. (b) Longitudinal turbulent intensity. (c) Lateral turbulent intensity. (d) Reynolds stress. ○, $T = 1.50$; △, $T = 1.75$; □, $T = 2.00$.

equivalent time-averaged turbulent quantities in the current Lagranian coordinates are obtained by taking the space average over quantities that are located with equal spacing in x but have a common y-coordinate at a particular instant. Aref and Siggia (1980) used the same method for computing the equivalent time-averaged quantities in the study of a typical vortex pair by the vortex-in-cell method. Some basic theoretical considerations of turbulent shear flow, such as statistical homogeneity along the shear layer, asymptotic behavior and self-preservation, were also computed in their study. In this simulation these quantities are also calculated to check the quality of the flow solutions.

In checking the self-preservational aspect of the flow, one needs to scale all the velocities by ΔU and the length dimension across the shear layer by the time-dependent momentum thickness, $\theta(T)$, which is defined according to Browand & Weidman (1976) as

$$\theta(T) = \int_{-\infty}^{\infty} \left[\frac{1}{4} - \frac{u(y, T)}{\Delta U}\right] \mathrm{d}y. \qquad [15]$$

The variation of $\theta(T)$ with respect to time is shown in figure 5, and it is approximately linear during the vortex-pairing period.

The mean velocity distribution at different y-locations across the shear layer is calculated by following averaging technique, based on the equivalent time-averaged concept discussed above:

$$\bar{u}(y, T) = \frac{1}{m} \sum_{i=1}^{m} u(x_i, y, T) \qquad [16]$$

and

$$\bar{u}(y, T) = \frac{1}{m} \sum_{i=1}^{m} v(x_i, y, T), \qquad [17]$$

where m is the number of points used in the averaging and is equal to 100. Figure 6(a) shows the calculated mean velocity profiles at three different times. The boundary conditions, i.e.

$$\lim_{y \to \pm\infty} \bar{u}(y, T) = \mp U, \qquad [18]$$

are clearly satisfied. The self-preservation characteristic of the flow is verified in figure 6(a) where the mean velocity is scaled by ΔU and the distance across the shear layer by $\theta(T)$. Velocity at three different times all converge into one curve. This result is also in good agreement with those of Aref & Siggia (1980), Browand & Weidman (1976) and Stuart (1967). The experimental values of Browand & Weidman (1976) are shown (●) for comparison purposes.

The longitudinal and transversal turbulence intensities are obtained by the following equations:

$$(\overline{u'^2})^{1/2} = \sqrt{\frac{1}{m} \sum_{i=1}^{m} [u(x_i, y, T) - \bar{u}(y, T)]^2} \qquad [19]$$

and

$$(\overline{v'^2})^{1/2} = \sqrt{\frac{1}{m} \sum_{i=1}^{m} [v(x_i, y, T) - \bar{v}(y, T)]^2} \qquad [20]$$

The results for the above turbulent quantities are shown in figures 6(b), (c). It is seen that some scattering of the calculated data is present in the region near the center of the shear layer. Similar scattering is also found in the simulation of Aref & Siggia (1980) even though they used 4096 vortices in their calculation. The self-preservation is valid in these distributions except near the center region.

Even though the current results of turbulence intensities compare well with the numerical results of Aref & Siggia (1980), but the experimental results of Browand & Weidman (1976) indicate lower magnitudes in turbulence intensites. It has been a uniform trend in many reported results that turbulence intensities calculated in numerical simulations by the discrete vortex method are always somewhat larger than those measured in experiments. It is of interest to note that the magnitude of $(\overline{u'^2})^{1/2}$ is always less than that of $(\overline{v'^2})^{1/2}$, which agrees with the experimental measurements of Browand & Weidman (1976).

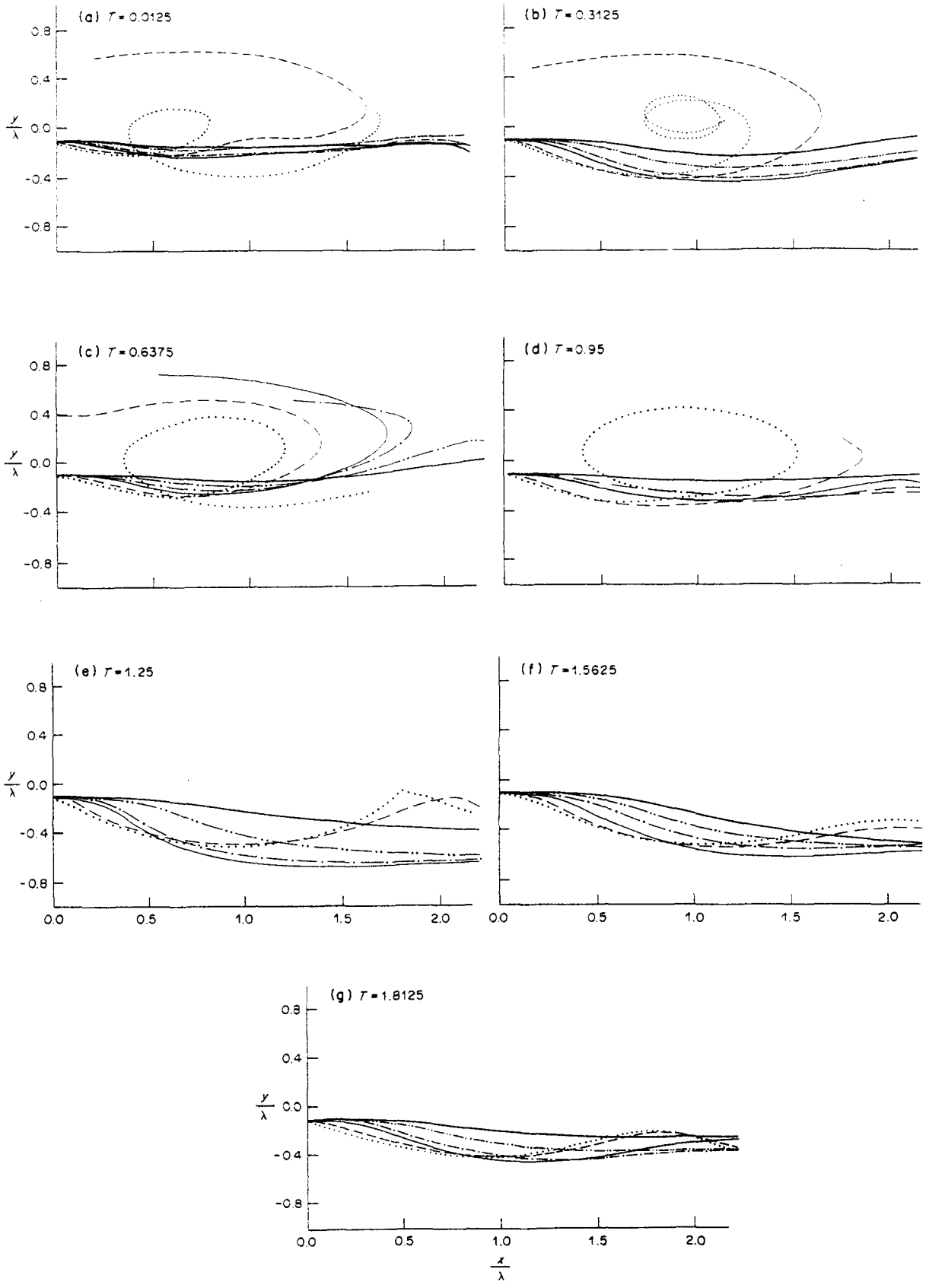

Figure 7. Trajectories of particles with different release times from a fixed point. ····, St = 0.01; – – –, St = 0.1; ——, St = 0.5; –·–, St = 0.8; –··–, St = 2; ——, St = 5.

The Reynolds stress, another important quantity of turbulent flow, is calculated by the following equation:

$$\overline{u'v'} = \frac{1}{m}\sum_{i=1}^{m}[u(x_i, y, T) - \bar{u}(y, T)][v(x_i, y, T) - \bar{v}(y, T)]. \quad [21]$$

Since the gradient of the mean velocity distribution $d\bar{u}(y, T)/dy$ is negative, the Reynolds stress should remain positive. The result is shown in figure 6(d), which agrees well with that of Aref & Siggia (1980).

Based on the above results and the comparisons with experiments and other numerical results, we believe that the flow-field simulations are reasonably accurate.

Next we discuss the interactions of particles with this large-scale vortex pair, especially the effect of the pairing process on the particle lateral displacement. First, some typical particle trajectories are given in figures 7(a–g) for particles released into the flow field at different stages of the vortex-pairing process. The other parameters which need to be specified in obtaining the results if figures 7(a–g) are given as:

$$\mathrm{Re} = 20{,}000, \textit{ flow-field Reynolds number};$$

$$(x, y) = (0, -0.1), \textit{ particle starting position};$$

$$(u, v) = (1, 0), \textit{ particle starting velocity};$$

$$\gamma_\rho = 1500, \textit{ particle/fluid density ratio}.$$

Based on figures 7(a–g), we may summarize the important findings as follows:

1. In figure 7(a), particles released at $T = 0.0125$ interact mostly with the flow field during the pre-pairing period, when the two vortex structures still have separate identities but some interactions between them have begun. It is evident that the trajectories of the particle with $\mathrm{St} = 0.01$ are similar to the flow streamlines. Therefore particles with $\mathrm{St} = 0.01$ are assumed to represent the fluid particles in the dispersion study and their dispersion is used as a reference for comparing the dispersion of other particles. It is noted that the Stokes number is equal to the dimensionless diameter of the particle when Reynold number and γ_ρ are held constant, as in the cases presented in figures 7(a–g). As to the flow in the pre-pairing stage, the vortex structures enhance the particle displacement only for relatively small particles [$\mathrm{St} \leqslant O(0.1)$ in this analysis].
2. Particles released at $T = 0.3125$ interact with the flow field during the later stages of pre-pairing as well as during the early stages of pairing. The effects of the vortex structure are similar to those in figure 7(a) but the displacement is increased from 0.2 to 0.4 for $\mathrm{St} = 0.1$ as far as the highest point of the trajectory is considered.
3. The particles will interact with the flow field during most of the pairing process if they are released to the flow at $T = 0.6375$. As seen in figure 7(c), the pairing process clearly has the strongest effect on the particle lateral displacement. As shown by the trajectories, the flow during pairing seem to have the maximum power of entraining particles and setting them into vortical motion. Only particles with $\mathrm{St} = 2$ and 5 were seen to penetrate through the vortex structure without being entrained into circular motion, particles will then be flung out of the structures from various different positions depending on their Stokes numbers. The maximum lateral displacement for the cases shown in figure 7(c) is achieved by the particle with $\mathrm{St} = 0.5$. For the rest of the particles, the lateral displacement increases with increasing Stokes number for particles with $\mathrm{S} < 0.5$, while it decreases with increasing Stokes number for particles with $\mathrm{St} > 0.5$. This interesting finding is explained based on the balance between particle inertia and the drag force exerted by the flow. This balance determines at what point a particle gets flung out of the pairing flow loop. We will discuss this point again in more detail.

4. For the particles interacting with the flow field in the latter stages of the pairing process and post-pairing, the magnitudes of the displacement as shown in figure 7(d) are similar to those shown in figure 7(a).
5. Particles released after $T = 1.25$ generally interact with the post-pairing flow field. It can be seen that the displacement is rather limited for all Stokes numbers.

We learn from these trajectories that particles with smaller Stokes numbers tend to follow the streamlines, while those with larger Stokes numbers tend to follow an almost straight path propelled by their large initial inertia. Intermediate particles will be entrained by the flow initially, but they will be flung out of the looping flow field at some point, depending on their inertia/drag ratio. Also, it seems reasonable to conclude that the flow field during the pairing process is capable of producing large particle dispersion, as a result of the strong entrainment power which induces the particles into vortical motion and then flings them out of the vortex structures.

For the purpose of quantifying the dispersion characteristics of an evolving vortex structure during pairing process, the displacement of particles with respect to the fluid displacement is present in figures 8(a–e). The vertical coordinate is used to express the ratio of the maximum lateral displacement of each particle with a specific Stokes number relative to its starting position to that of the particle with St = 0.01, which is assumed to represent the maximum displacement of the fluid particles, as discussed earlier. This ratio will indicate the particle displacement relative to the fluid displacement. Except in figure 8(e), all particles are released at $(0, -0.1)$. Figure 8(a) demonstrates the effects of various particle release times. Particles released at $T = 1.575$ and $T = 1.700$ are all affected by the pairing process as shown by the higher-than-unity portions of the curves. Particles released at $T = 1.825$ will interact with the post-pairing flow where the displacement of particles by the flow is much less extensive. For larger Stokes numbers, the particles also are not significantly affected by the flow. Figure 8(b) represents the effects of the density ratio. For $St < 1$, variation in γ_ρ does not seem to change the displacement ratio at all. Some small changes are seen for large Stokes numbers. This can be explained by reviewing [14], which defines the relationship between St, γ_d, γ_ρ and Re. In figure 8(b), the Reynolds number is held constant, any change in γ_ρ will result in different γ_d for a given Stokes number; γ_ρ represents the inertia ratio while γ_d represents the drag ratio. Because the product of γ_ρ and γ_d^2 is a constant for the case in figure 8(b), the variation of γ_ρ is roughly offset by the corresponding change in γ_d for small, but not for larger, Stokes numbers.

The effects of Reynolds number are shown in figure 8(c). For $St < 1$, Reynolds number does not make any difference in the displacement ratio. Only slight effects are seen for large Stokes numbers. In figure 8(d), particles are assigned different initial velocities. Higher initial velocity seems to decrease the displacement, as a result of the increased inertial. When particles are released at different starting points, as shown in figure 8(e), the displacement ratio does not seem to be sensitive to the starting locations as long as they are close the mid-plane of the vortex structures.

Based on the results of the above single-source, continuous-released analysis, it is clear that the dispersion is strongly dependent on the stage of the pairing process at which the particle is released. Therefore it is considered undesirable to use a point source in the following statistical analysis which is designed to study the general dispersion capability of the entire pairing process. Instead, all particles are initially placed at $y = 0$ with equal spacing between adjacent particles. The initial velocities of all particles are set equal to zero. Since we are only concerned with lateral dispersion (y-direction), the y-coordinate of each particle is recorded at each time step for further analysis. The distributions of particles as a function of y at various times and different Stokes numbers are presented in figures 9(a–j). The ordinate indicates the number of particles (n) in the range of $(y - \frac{1}{2}\Delta y, y + \frac{1}{2}\Delta y)$ divided by the total particles (N) in the system. In our analysis, $\Delta y = 0.1$ and $N = 100$.

In general, for small times the particle distribution profiles all resemble the Gaussian distribution. As time increases, the particle distribution profiles evolve into different shapes which depend strongly on the Stokes number. The distribution patterns may be categorized into three groups. For those particles with $St < 0.1$, the particle distributions will evolve from the initial Gaussian shape into a double-peak profile which is symmetric with respect to $y = 0$. This is as expected because the particles will follow the streamlines closely for the small Stokes numbers. A similar pattern results when particles were replaced by dye particles (fluid markers). For large particles

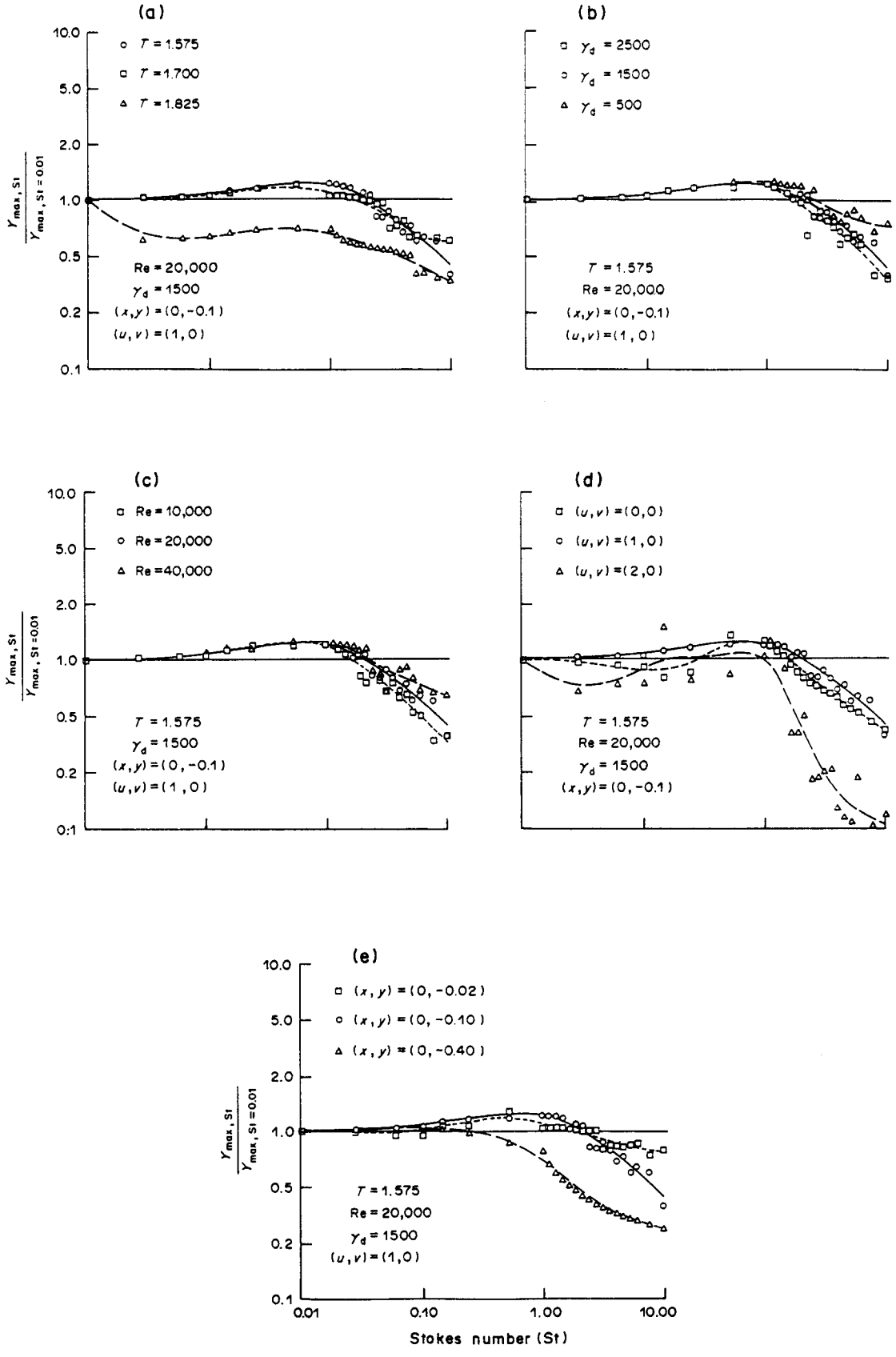

Figure 8(a–e). Effects of various parameters on the ratio of particle maximum displacement to the fluid maximum displacement. (a) Particle release times. (b) Density ratio. (c) Flow Reynolds number. (d) Initial particle velocity. (e) Particle source location.

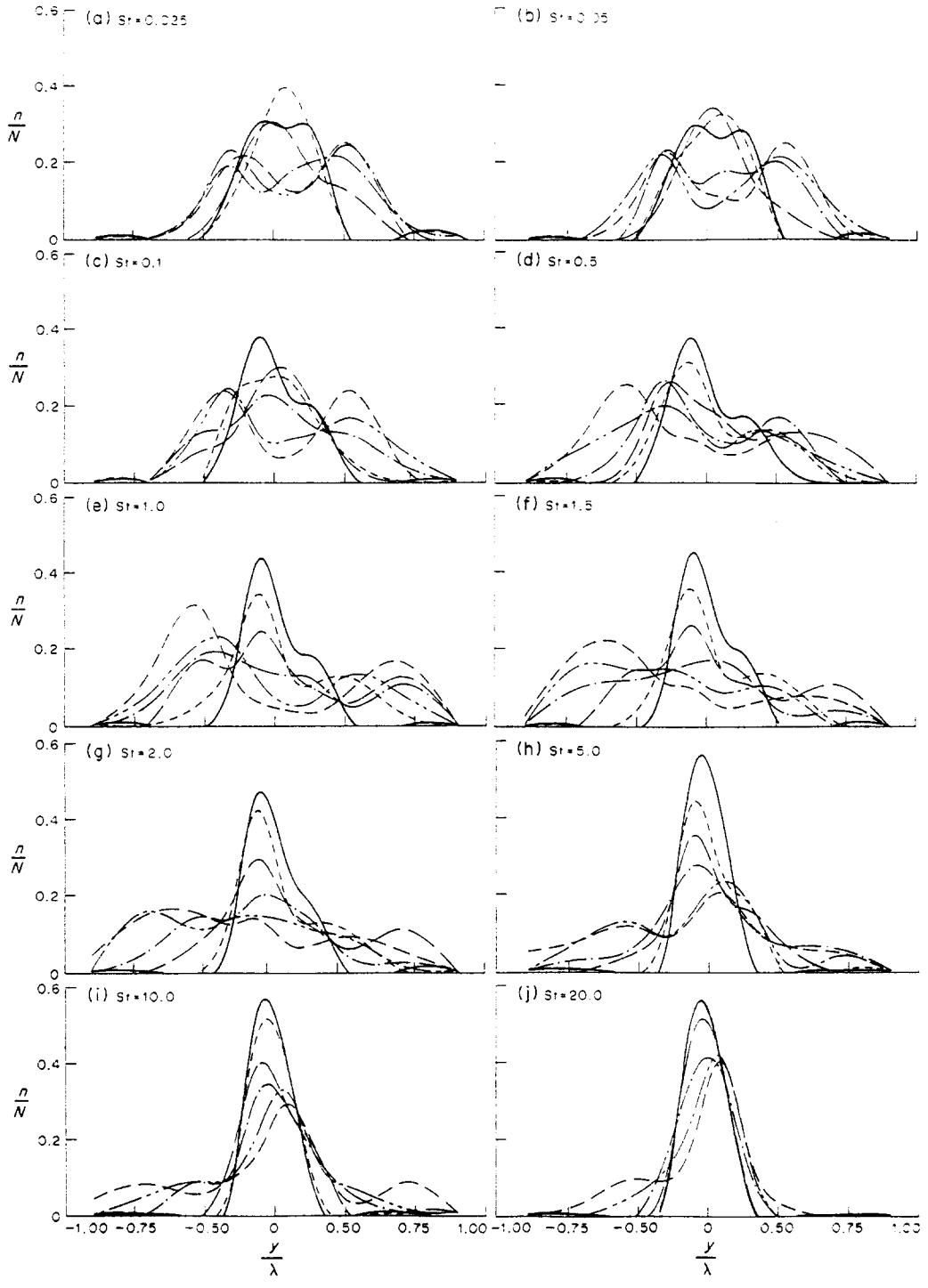

Figure 9(a–j). Lateral distribution of particles at various times. ——, $T = 1.0$; - - -, $T = 1.5$; – – –, $T = 2.0$; —·—, $T = 2.5$; ——··——, $T = 3.0$; – – –, $T = 3.5$.

(St $\geqslant$ 5), the distributions remain Gaussian all the time and it means that the particles are not affected significantly by the vortex structures. The lateral dispersion for this group is less than that of the first group. The third group consists of particles with intermediate Stokes numbers ($0.5 \leqslant \mathrm{St} \leqslant 5$). If we compare figure 9(a), considered to be the case of particles closely following streamlines, with figure 9(e) or figure 7, we may conclude that the lateral spread is most extensive for the third group. Particles are seen outside the vortex structures, i.e. they have been flung out

of the vortex loops as evidenced in the single-point-source analysis [figure 7(c)]. It seems that there exists a specific range of Stokes number, at which optimal lateral dispersion may be achieved.

Next we attempt to seek a correlation between the current discrete approach and the Fickian diffusion concept. The particle dispersion with respect to the mean displacement Y_m is defined as

$$D_y^2(T) = \frac{1}{N}\sum_{i=1}^{N}(Y_i - Y_m)^2 \qquad [22]$$

and

$$Y_m = \frac{1}{N}\sum_{i=1}^{N} Y_i, \qquad [23]$$

where Y_i is the lateral displacement of particle at time T, which is also the y-coordinate of the particle location at time T. The average is taken over all the particles in the system. The dispersion curves of three distinct ranges of particle Stokes number, as discussed above, are shown in figures 10(a–c). For large particles, the dispersion curves are approximately proportional to T^2. From the study of particle dispersion in homogeneous turbulent flow field (Hinze 1975), it is known that

$$D_y^2(T) = V'^2T^2 \qquad [24]$$

for short diffusion time T, in which V'^2 is the particle turbulence intensity and this particle autocorrelation coefficient is $\cong 1$. Since particles with large Stokes numbers are not affected significantly by the flow field, it is not surprising to find that the dispersion vs time curves as shown in figure 10(a) for particles with $St > 5$ may be represented by [24]. It is suggested that for large Stokes number cases, the large-scale structures may look like homogeneous turbulent flows to the particles because of their large size, high inertia forces and short residence time in the system. In figures 10(b, c) we show the time-dependent dispersion for intermediate and small Stokes numbers. Again the idea is that the dispersion of small Stokes number particles should be closely related to the fluid dispersion of the vortex structure because the particles closely follow the streamlines. Due to the similarity in the transport mechanism, the momentum thickness of the shear layer shown in figure 5 may be used to explain the following particle dispersion process for particles with small Stokes numbers. During vortex pairing, the rate of increase is at its highest and an apparent decrease after the pairing process is present in both figures 5 and 10(c). Figure 10(b) shows the transition phenomenon between large and small Stokes numbers. The magnitude of dispersion is also large, as expected. Figures 10(d–f) show the effects of the variation of γ_ρ on particle dispersion. Similar to the displacement ratio discussed above, the effect of λ_ρ becomes increasingly important as the Stokes number gets larger. Almost identical trends are obtained when the Reynolds number is changed from 10,000 to 40,000. The results are plotted in figures 10(g–i).

We would like to emphasize that in this study we investigated specifically particle dispersion due to the "pairing process", which was discovered and has been verified by many experimentalists in turbulent shear flows. However, it is difficulty to perform any measurement of particle dispersion induced by a specific vortex pair in an experiment. Therefore, we have not found any published results of particle dispersion for comparison with the results of this work.

4. CONCLUSION

Numerical solutions for particle dispersion in a vortex-pairing flow are presented. The discrete vortex simulations of the local pairing phenomenon show reasonble comparison with the experimental flow visualization pictures. Qualitatively speaking, the computed mean velocity, turbulent intensities and Reynolds stress were also shown to be comparable to the experimental values and to numerical results obtained by other methods. In the analysis of the particle lateral displacement from a point source in the pairing flow, it is found that through examining the particles' trajectories, the vortex flow during pairing shows a distinctively higher capability to entrain the particles and disperse them more than both the pre-pairing and the post-pairing flows. This finding seems to be consistent with published results, which indicate that the pairing process is solely responsible for the entrainment of the ambient fluid and therefore accounts for the growth of the shear layer. Using fluid particle displacement as a reference, particles with small Stokes

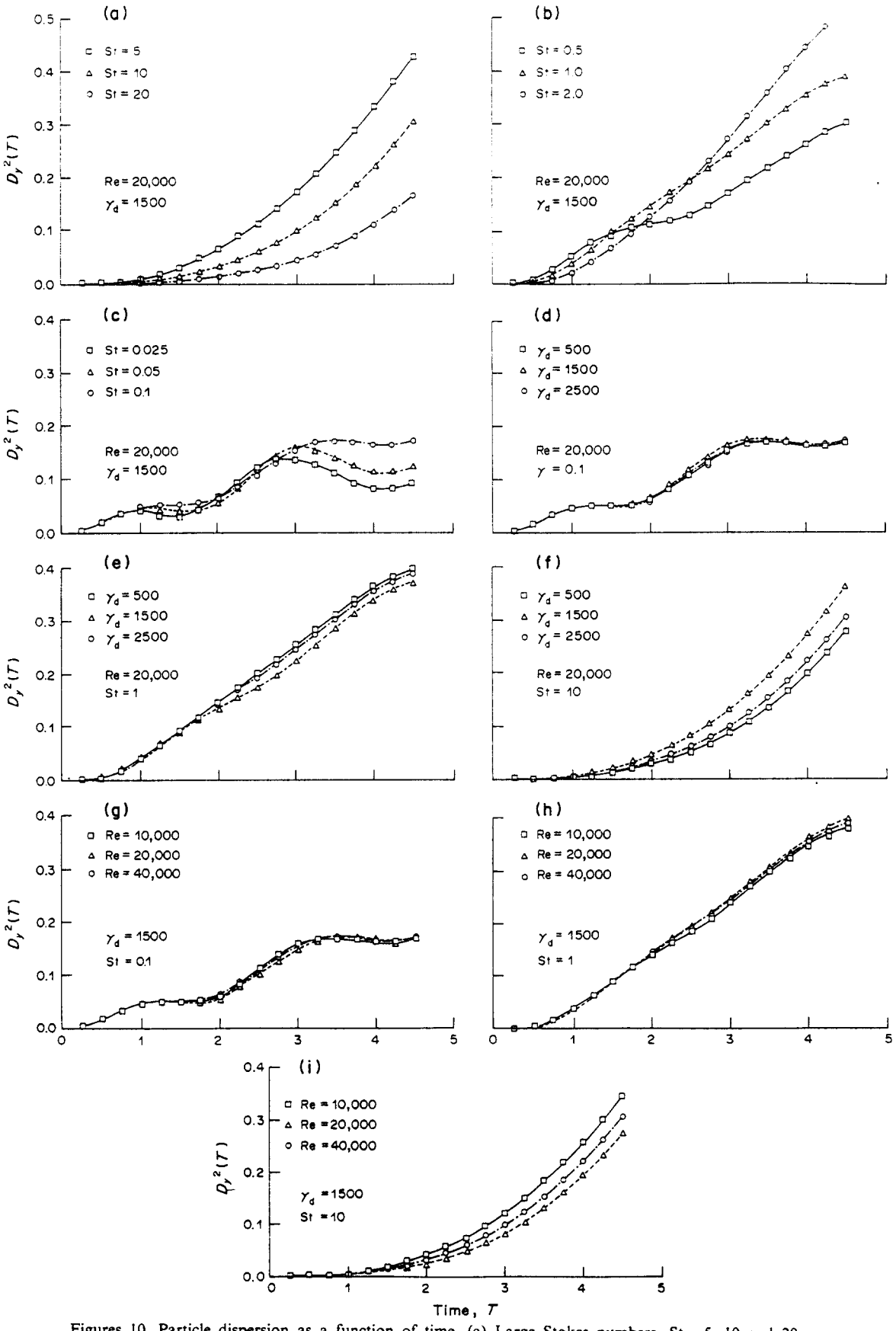

Figures 10. Particle dispersion as a function of time. (a) Large Stokes numbers, St = 5, 10 and 20. (b) Stokes numbers close to unity, St = 0.5, 1 and 2. (c) Small Stokes numbers, St = 0.025, 0.05 and 0.1. (d) Effect of density ratio on dispersion, St = 0.1. (e) Effect of density ratio on dispersion, St = 1. (f) Effect of density ratio on dispersion, St = 10. (g) Effect of Reynolds number on dispersion, St = 10. (i) Effects of Reynolds number on dispersion, St = 10.

numbers are displaced similarly to the fluid particles, particles with large Stokes numbers are displaced less than fluid particles. Particles with intermediate Stokes numbers, i.e. St = 0.5 to 5, are displaced more than fluid particles. For the case of a distributed initial line source, all particle distribution profiles resemble the Gaussian distribution in the early development of the pairing process. As time goes on, for small Stokes numbers, the particle distributions gradually evolve into an symmetrical double-peak profile. For intermediate Stokes numbers, the distributions are hard to generalize but they all show wider lateral spread. Similar trends in dispersion phenomena to those with a single point source are also found for the distributed source case.

It should be emphasized that the particle dispersion results presented in this study should be considered to be of first order in circumstances when small-scale three-dimensional disturbances, which may show up after a transition point in a mixing layer, or forces other than drag force, could affect the particle dispersion up to second order.

Based on this numerical study, we suggest that there seems to exist a specific range of the Stokes number at which optimal dispersion of particles in large-scale turbulent shear flows may be achieved.

Acknowledgements—Major portions of this research were accomplished when both authors were participants in the NASA-Lewis Research Center 1985 Summer Faculty and Graduate Student Fellowship Program. We appreciate both the financial support and use of the computing facilities. Various assistance provided by Mr Dan Bulzan is also noted. Free computing time from the Computing Center of Washington State University was important in finishing this project.

REFERENCES

ACTON, E. 1976 Large-eddies in a two-dimensional shear layer. *J. Fluid Mech.* **87,** 561–591.

ACTON, E. 1980 A modeling of large eddies in an axisymmetric jet. *J. Fluid Mech.* **98,** 1–31.

AREF, H. & SIGGIA, E. 1980 Vortex dynamics of two-dimensional turbulent shear layers. *J. Fluid Mech.* **100,** 705–737.

ASHURST, W. T. 1979 Numerical simulation of turbulent mixing layers via discrete vortex dynamics. In *Turbulent Shear Flow I* (Edited by DURST *et al.*), pp. 402–413. Springer, New York.

BATCHELOR, G. K. 1956 *Theory of Homogeneous Turbulence.* OUP, Oxford.

BATCHELOR, G. K. 1956 Diffusion on free turbulent shear flows. *J. Fluid Mech.* **3,** 67–80.

BROWAND, F. K. & TROUTT, T. R. 1980 A note on the spanwise structures in two-dimensional mixing layer. *J. Fluid Mech.* **97,** 771–781.

BROWAND, F. K. & TROUTT, T. R. 1985 The turbulent mixing layer: geometry of large vortices. *J. Fluid Mech.* **158,** 489–509.

BROWAND, F. K. & WEIDMAN, P. D. 1976 Large-scales in the developing mixing layer. *J. Fluid Mech.* **97,** 127–144.

BROWN, G. L. & ROSHKO, A. 1974 Density effects and large-scale structure in turbulent mixing layer. *J. Fluid Mech.* **64,** 775–816.

CHORIN, A. J. 1973 Numerical study of slightly viscous flow. *J. Fluid Mech.* **57,** 785–796.

CLIFT, H., GRACE, J. R. & WEBER, M. E. 1978 *Bubbles, Drops, and Particles.* Academic Press, New York.

CROWE, C. T. 1982 Review—numerical models for dilute gas–particle flows. *J. Fluid Engng ASME* **104,** 247–303.

GORE R. A., CROWE, C. T., TROUTT, T. R. & RILEY, J. J. 1985 A numerical study of particle dispersion in large-scale structures. *ASME Publication HTD*, Vol. 47; *Multiphase Flow and Heat Transfer*, BK No. 600304.

HINZE, J. O. 1975 *Turbulence*, 2nd edn. McGraw-Hill, New York.

INOUE, O. 1985 Vortex simulation of a turbulent mixing layer. *AIAA Jl* **23,** 367–372.

INOUE, K. & TAKAMI, H. 1985 Study of turbulent wake behind a bluff body body by vortex method. In *Proceedings of IUTAM Symposium on Turbulence and Chaotic Phenomena in Fluids* (Edited by TATSUMI, T.). North-Holland, Amsterdam.

KUWAHARA, K. & TAKAMI, H. 1983 Study of turbulent wake behind a bluff body by vortex method. In *Proceedings of IUTAM Symposium on Turbulence and Chaotic Phenomena in Fluids* (Edited by TATSUMI, T.). North-Holland, Amsterdam.

LAMB, H. 1945 *Hydrodynamics*, 6th edn. Dover, New York.

ROSENHEAD, L. 1932 Formulation of vortices from a surface of discontinuity. *Proc. R. Soc. Lond.* **A134,** 170–192.

STUART, J. T. 1967 On finite amplitude oscillations in laminar mixing layers *J. Fluid Mech.* **29,** 417–440.

TAYLOR, G. I. 1921 Diffusion by continuous movements. *Proc. Lond. math. Soc.* **20,** 196.

WINANT, C. D. & BROWAND, F. K. 1974 Vortex pairing, the mechanism of turbulent mixing mixing layer growth at moderate Reynolds numbers. *J. Fluid Mech.* **63,** 237–255.

YULE, A. J. 1980 Investigation of eddy coherence in jet flows. *Lecture Notes Phys.* **136,** 188–207.